JTTEE5 24:1038–1045
DOI: 10.1007/s11666-015-0248-9
1059-9630/$19.00 © ASM International

Characterization of Plasma Jet in Plasma Spray-Physical Vapor Deposition of YSZ Using a <80 kW Shrouded Torch Based on Optical Emission Spectroscopy

Qing-Yu Chen, Xiao-Zhuang Peng, Guan-Jun Yang, Cheng-Xin Li, and Chang-Jiu Li

(Submitted January 7, 2015; in revised form March 19, 2015)

During plasma spray-physical vapor deposition (PS-PVD) of yttria-stabilized zirconia (YSZ) coatings, evaporation of the YSZ powder is essential, but quite difficult when using a commercial <80 kW plasma torch. In this study, a shrouded plasma torch was examined to improve the YSZ evaporation. The plasma characteristics were diagnosed using optical emission spectroscopy. Results showed that the electron number density in the plasma jet was maintained at an order of magnitude of 10^{14} cm^{-3}, indicating local thermal equilibrium of the plasma jet. Compared with a conventional torch, the shrouded torch resulted in much higher plasma temperature and much lower electron number density. With the shrouded torch, more energy of the plasma was transferred to the YSZ material, leading to more evaporation of the YSZ powder and thereby a much higher deposition rate of the YSZ coating. These results show that use of a shrouded torch is a simple and effective approach to improve the evaporation of feedstock material during PS-PVD.

Keywords optical emission spectroscopy, PS-PVD, shrouded plasma torch, yttria-stabilized zirconia

1. Introduction

During conventional atmospheric plasma spraying (APS), the powder is injected into a plasma jet to be melted, accelerated, and finally deposited onto the substrate surface in the form of lamellar splats (Ref 1–3). It is well known that the temperature at the center of the plasma jet can be >10,000 K, which is much higher than the boiling point of any material. Therefore, powder evaporation can be found in APS (Ref 4–6), although evaporation of the spray powder is not necessary.

Plasma spray-physical vapor deposition (PS-PVD), a new technique combining the merits of atmospheric plasma spraying (low cost and high deposition rate) and electron beam-physical vapor deposition (EB-PVD) to deposit an YSZ coating with high strain tolerance and high thermal shock resistance (Ref 7), has been developed in recent years (Ref 8, 9). It also bridges the coating thickness gap between physical vapor deposition and conventional plasma spray technology (Ref 10). In the PS-PVD process, the plasma jet expands to more than 2 m long and 200–400 mm in diameter (Ref 11). With this enlarged plasma jet, the spraying materials (metal or ceramic) should be, at least partially, evaporated in the plasma jet and deposited in the form of gaseous phase including atoms or clusters (Ref 12).

At very low pressures, such as 50–200 Pa, the density of the plasma jet is significantly decreased in the enlarged jet. Effective evaporation of powder is a great challenge, since the low pressure decreases the heating performance of the plasma jet for the spray powder. The current solution mainly includes two aspects. Firstly, a super-high-power (e.g., 180 kW) plasma torch is utilized to improve the material evaporation (Ref 13, 14). Secondly, agglomerated powder, which can be fragmented into fine primary particles, has to be used to improve the evaporation of powder (Ref 15). This significantly limits the development of PS-PVD and its future industrial applications. In fact, based on analysis of the heating process, the thermal energy used to evaporate the powder is a very small fraction of the plasma power. This means that most of the thermal energy in the plasma jet is lost during the PS-PVD process. Therefore, it is of significant importance to enhance the energy efficiency by examining the evaporation behavior of the spray powder in the plasma torch.

Besides columnar YSZ, composite YSZ with both columnar and lamellar structure is more interesting when using PS-PVD, for example, for thermal barrier coating (TBC) deposition. The columnar structure results from vapor deposition, whereas the lamellar structure results from liquid droplets. Therefore, the fraction of evaporation should be freely controllable to tailor the coating

Qing-Yu Chen, Xiao-Zhuang Peng, Guan-Jun Yang, Cheng-Xin Li, and **Chang-Jiu Li**, State Key Laboratory for Mechanical Behavior of Materials, School of Materials Science and Engineering, Xi'an Jiaotong University, Xi'an, Shaanxi 710049, P.R. China. Contact e-mails: ygj@mail.xjtu.edu.cn and licj@mail.xjtu.edu.cn.

structure, which relies on understanding or control of the evaporation of feedstock.

Plasma emission spectroscopy, as a method having no interference, can be used for analysis of a variety of plasma physical characteristics, such as plasma electron temperature, electron number density, excitation temperature, and even some kinetic processes. In view of the high temperature of the plasma, the continuous radiation spectrum can be used for measurement of electron temperature (Ref 16). The Stark effect in the linear spectrum can be used for measurement of electron number density (Ref 17). The intensity distribution of the linear spectrum can be used in diagnosis of the excitation temperature (Ref 18). Optical emission spectrometry (OES) can be used in the PS-PVD process to diagnose the characteristics of the plasma jet (Ref 19). Recently, Mauer et al. (Ref 15, 20) also used the Boltzmann plot and Stark broadening to calculate the excitation temperature and electron number density in a plasma jet. The characteristic of a plasma jet at low pressure is different from that of a plasma jet at atmospheric pressure. Under the low-pressure condition, the plasma jet expands, resulting in lower electron number density and larger high-temperature zone (Ref 21). The plasma jet length is significantly increased as the pressure is reduced (Ref 14).

In the present study, a shrouded torch with a commercially <80 kW power was used to restrict the expansion of the plasma jet and improve its heating effect on the spray powder. Optical emission spectroscopy was used to examine the plasma characteristics and clarify the enhanced evaporation of the spray powder.

2. Experimental

2.1 Materials and Coating Deposition

Agglomerated 7 wt.% yttria partially stabilized zirconia powder (M6700, Sulzer-Metco, Switzerland) with particle size below 25 μm was used as feedstock powder in this study. The primary size of the powder was about 130 nm. To fully utilize the plasma energy to evaporate the feedstock, the powder was injected into the plasma internally within the spray nozzle. The alumina substrate was polished and degreased before coating deposition.

A commercial plasma spray torch (F6, 80 kW class, GTV, Germany) was mounted on a six-axis robot (Lab-modified IRB 1600, ABB, Sweden) in a 10 m^3 vacuum chamber. The plasma spraying parameters used in this study are presented in Table 1. The chamber pressure was maintained at 100 Pa during spraying.

2.2 Characterization of Coating

To eliminate interference from liquid droplets, the coating was deposited in the direction parallel to the plasma jet. Owing to inertia, the droplets were not able to deposit in this direction. The surface and cross-section morphologies of coatings were observed by field-emission scanning electron microscopy (MIRA3 LMH, TESCAN, Czech Republic).

Table 1 Plasma spraying parameters used in this study

Parameter	Value
Arc power, kW	45
Arc current, A	600
Ar gas flow, slpm	40
H_2 gas flow, slpm	8
Spray distance, mm	50–350
Powder feed rate, g/min	0.5

2.3 Diagnosis of Plasma Condition by OES

Optical emission spectrometry was used to examine the condition of the plasma jet during the YSZ deposition process. The spectrometer used was an imaging triple-grating monochromator/spectrograph (Acton SP2750, Princeton Instruments, USA). To clearly describe the plasma state, a Cartesian coordinate system was proposed, as shown in Fig. 1. The Z axis was along the axis of the spray torch with origin at the nozzle exit of the torch for both cases, i.e., with or without shroud. The light emission from the plasma jet was first collected by a lens (FC-446-030, Andor Technology, British), then transported to the spectrometer by an optical fiber. The detecting region is a cylinder, as shown in the inset in Fig. 1. The details of the shroud, which was water cooled, are also shown in the inset in Fig. 1. For data acquisition, a grating with 300 grooves/mm was selected to diagnose the light emission from the plasma; the resolution of the spectrometer was 0.058 nm. The spectral region from 300 to 1000 nm was selected. The wavelength positions of the spectrometer were calibrated using a standard mercury lamp before detection. Generally, Abel inversion is used to reconstruct the spatial plasma temperature to obtain the central characteristics of the plasma jet, through a deconvolution of the measured two-dimensional projections of the integrated intensities. However, the powder feeding was axial to the plasma torch, possibly resulting in a non-axisymmetric distribution of plasma temperature. Thus, the spectra were not Abel inverted. The spectra were tested three times to obtain the average value and standard error.

2.4 Examination of Electron Number Density

In this study, both the plasma temperature and electron number density of the plasma jet were examined. The electron number density was estimated by using the Stark broadening method, which is suitable for either equilibrium or nonequilibrium plasma (Ref 22, 23). In the present work, the spectral line (at wavelength of 486.1 nm) of the hydrogen Balmer series spectra was used to calculate the electron number density (Ref 24) as

$$\log n_e = 1.452 \log \Delta\lambda + 14.017, \quad \text{(Eq 1)}$$

where n_e (cm^{-3}) is the electron number density and $\Delta\lambda$ (Å) is the full-width at half-maximum (FWHM). In this

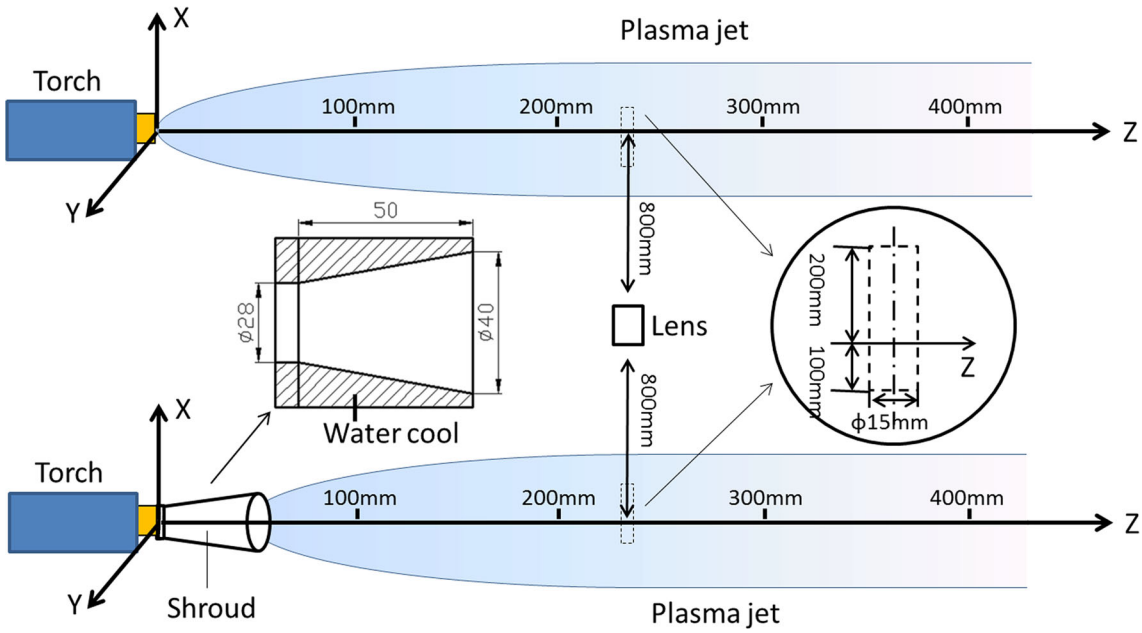

Fig. 1 Position diagram of plasma jet and emission detection

calculation, the spectral line was fit using a Voigt function, which is a convolution of a Lorentz and a Gauss function. Since only Stark broadening causes a significant Lorentzian contribution (Ref 20), the Lorentzian half-widths were used to calculate the electron number density.

2.5 Examination of Plasma Temperature

For a system in thermal equilibrium or local thermal equilibrium, the temperatures of electrons, ions, and atoms can be regarded as the same, and the double-line method (also known as the strength comparison method) can be used to measure the plasma temperature (Ref 25) using

$$\frac{I_{ji}}{I_{kl}} = \frac{\lambda_{kl} A_{ji} g_j}{\lambda_{ji} A_{kl} g_k} \exp\left(\frac{E_k - E_j}{k_B T}\right), \quad \text{(Eq 2)}$$

where I_{ji} (a.u.) is the spectral intensity generated via the transition from energy level j to i, I_{kl} (a.u.) is the spectral intensity generated via the transition from energy level k to l, λ_{ji} (nm) is the wavelength in the spectrum generated via the transition from energy level j to i, λ_{kl} (nm) is the wavelength in the spectrum generated via the transition from energy level k to l, A_{ji} (s^{-1}) is the Einstein spontaneous transition probability from energy level j to i, A_{kl} (s^{-1}) is the Einstein spontaneous transition probability from energy level k to l, g_j is the statistical weight of energy level j, g_k is the statistical weight of energy level k, E_j (eV) is the excitation energy of energy level j, E_k (eV) is the excitation energy of energy level k, and k_B is the Boltzmann constant. The light intensity for the selected H_β (486.1 nm) and H_α (656.3 nm) (Ref 26) signals can be measured experimentally, corresponding to I_{ji} and I_{kl}, respectively. The other parameters can be obtained from the National Institute of Standards and Technology (NIST) database (Ref 27). In this calculation, both evaluated emission lines belong to the hydrogen species. For the transitions k to l and j to i, l and i correspond to the same ground state (hydrogen atom), while k and j correspond to the excited state of H_α and H_β.

3. Results

3.1 Electron Number Density of Plasma Jet

The distribution of the electron number density is shown in Fig. 2. It can be found from Fig. 2a–c that the powder feeding exerts no influence on the electron number density, both with and without the shroud. In addition, the electron number density with the shroud is lower than that without the shroud. The electron number density without the shroud did not change as the spray distance (Z axis) was increased from 80 to 350 mm. It also did not change with axial location from 0 to 30 mm. However, the intensity of the spectra was too low to calculate the electron number density accurately when y became equal to 30 cm for Fig. 2c. This was perhaps because the intensity of the plasma jet was much lower in the region far from the center. However, with the shroud, the electron number density decreased significantly, from 4.1×10^{14} cm^{-3} to 2.4×10^{14} cm^{-3}, as the spray distance (Z axis) was increased from 80 to 350 mm along the axial center of the plasma jet (Fig. 2a). Figure 2d shows that the change of the electron number density for the shrouded torch was significant in the range of 80–170 mm in the axial direction and the range of 0–15 mm in the off-axial directions. It

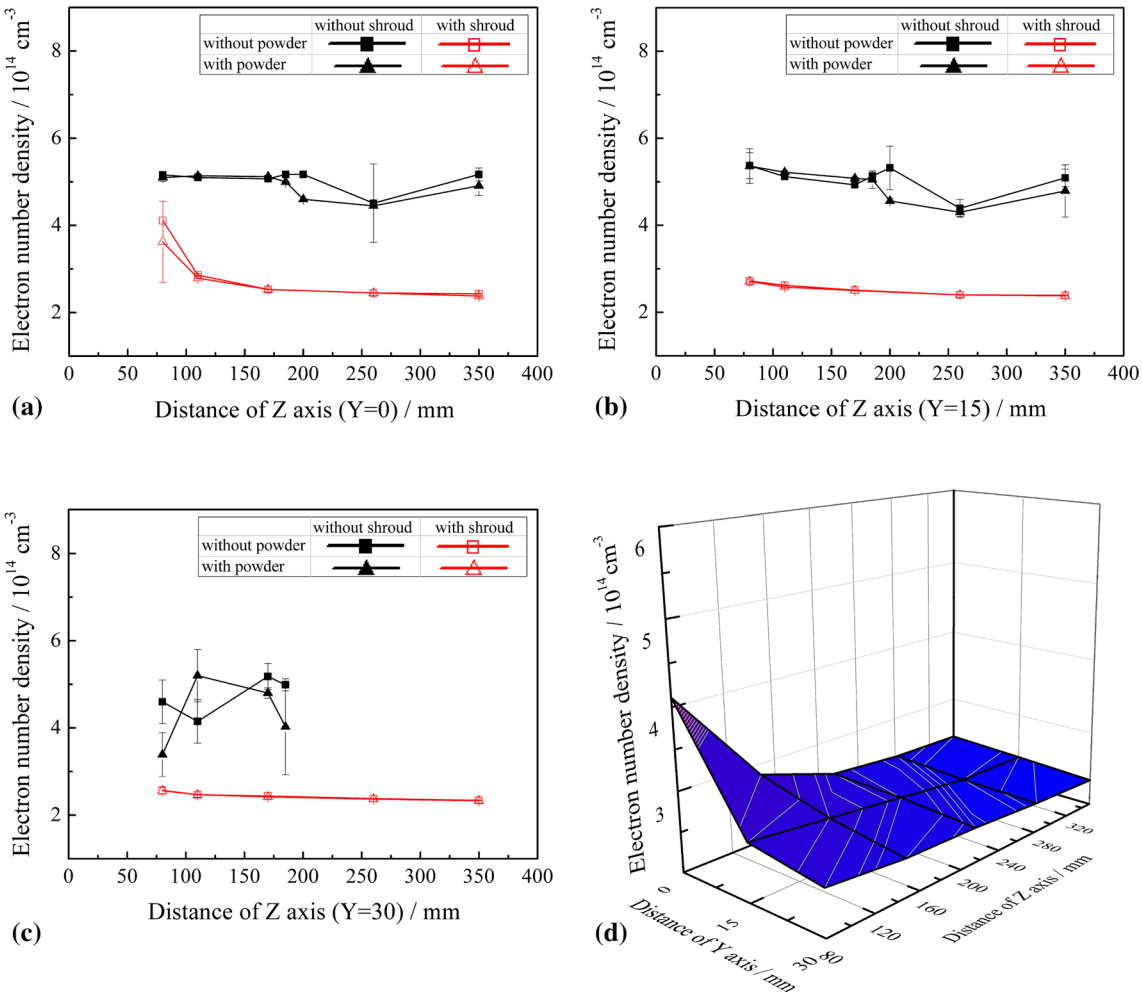

Fig. 2 Distribution of electron number density at (a) $Y = 0$ mm, (b) $Y = 15$ mm, and (c) $Y = 30$ mm. (d) Three-dimensional (3D) distribution with shroud and without powder

could be found that the electron number density decreased with increasing spray distance or divergence from the jet center.

3.2 Identification of Local Thermal Equilibrium

For examination of plasma temperature based on OES, the thermal equilibrium or local thermal equilibrium condition is required. In the PS-PVD approach, the plasma jet is composed of several gaseous constituents, i.e., neutral molecules and atoms, as well as ions and electrons in the plasma. Since the electrons are in a very high-energy state due to the electric charge in the plasma arc, they have a very different kinetic energy or temperature from the molecules and atoms. When the temperature of the above-mentioned species reaches the same level after sufficient energy exchange through collisions, the plasma jet can be defined as being in thermal equilibrium. According to the formula in Ref 28, shown in Eq 3, the time to achieve thermal equilibrium for the plasma jet is about 10^{20} s. However, the time from the localized plasma generation to its disappearance in the PS-PVD chamber is much less than 1 s. Therefore, there is insufficient time to achieve complete thermal equilibrium.

$$\tau_{\varepsilon}^{\mathrm{ei}} \approx \frac{\sqrt{2\pi} \cdot 3\pi\varepsilon_0^2 \cdot m_{\mathrm{e}}^{-1/2} m_{\mathrm{i}} T_{\mathrm{e}}^{3/2}}{n_{\mathrm{i}} Z^2 e^4 \ln \Lambda}, \qquad \text{(Eq 3)}$$

where $\tau_{\varepsilon}^{\mathrm{ei}}$ (s) is the time to achieve thermal equilibrium of electrons and ions, ε_0 is the vacuum dielectric constant, m_{e} (g) and m_{i} (g) are the electron mass and ion mass, T_{e} (K) is the electron temperature, n_{i} is the number concentration of ions, e is the elementary charge, Z is the partition function, and ln Λ is the Coulomb logarithm, whose value lies between 10 and 20.

For estimation in engineering applications, when the energy exchange between high-energy species (ions and electrons) and neutral species reaches a certain level, the plasma can be regarded as being in a state of local thermal equilibrium. Local thermal equilibrium is often defined as occurring when the electron number density of the plasma reaches a critical value. According to the simple formula given by Griem (Ref 29), shown in Eq 4, this critical electron number density can be estimated to be

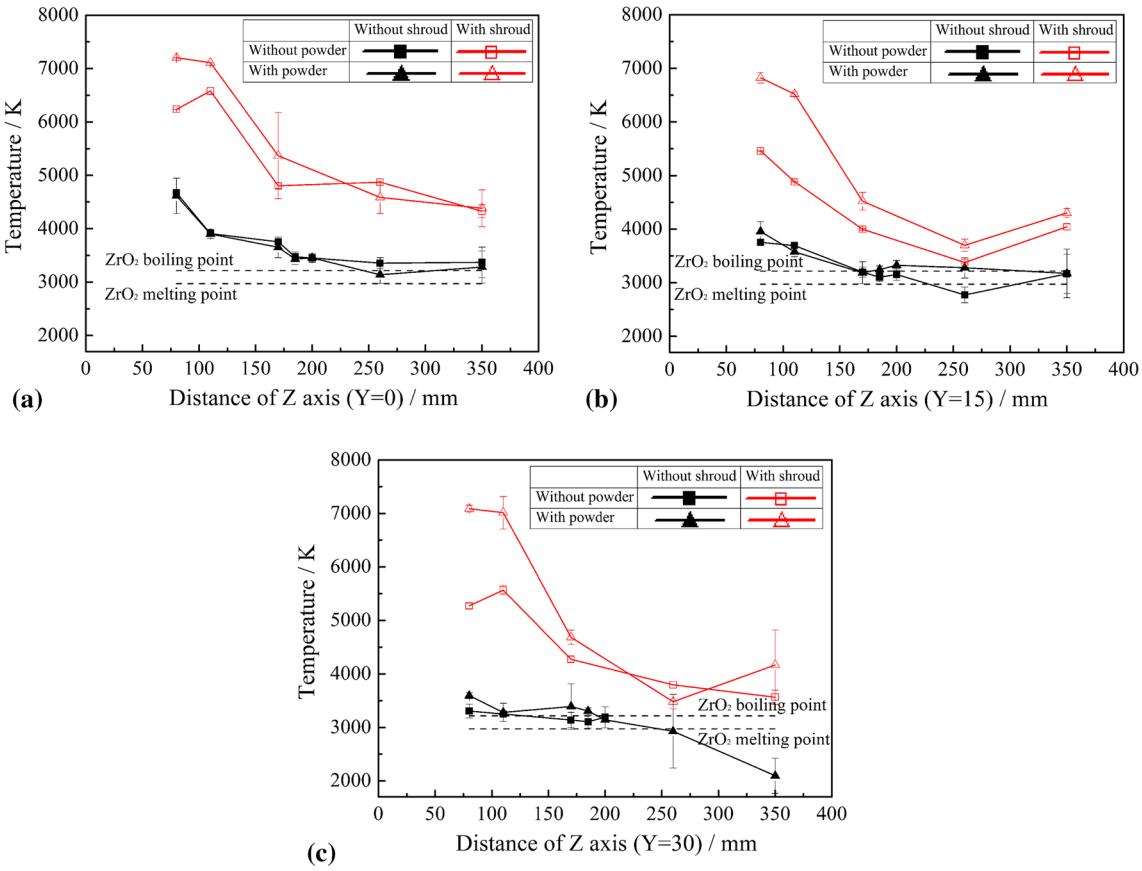

Fig. 3 Distribution of plasma temperature at: (a) $Y = 0$ mm, (b) $Y = 15$ mm, and (c) $Y = 30$ mm

4.2×10^{14} cm^{-3}, which is comparable to the electron number density shown in Fig. 2. Therefore, the plasma jet in this study can be regarded as being in a state of local thermal equilibrium.

$$n_e^* = 9 \times 10^{11} \times (E_2 - E_1)^3 T_e \ (\text{cm}^{-3}), \qquad \text{(Eq 4)}$$

where E_2 (eV) is the energy of the first excited state, E_1 (eV) is the energy of the ground state, and T_e (K) is the electron temperature.

3.3 Plasma Temperature

The distribution of plasma temperature is shown in Fig. 3. The plasma temperature was determined in this work on the basis of excitation, i.e., electron temperatures, since local thermal equilibrium was fulfilled, as discussed in section 3.2. The plasma temperature should be an average temperature imposed by the hot zone at the center of the plasma jet. The plasma temperature was not changed by the powder injection when taking the standard error bar into consideration. It could be found that the plasma temperature with the shroud was obviously higher than that without the shroud. It can be seen from Fig. 3a that the plasma temperature at the jet center gradually reduced along the Z axis from 80 to 350 mm. It can also be seen from Fig. 3b, c that the change of the plasma temperature along the Z axis at off-axis locations, e.g., for Y equal to 15 mm or 30 mm, was similar to at the center location.

3.4 Microstructure of Coating

Cross-sections of fractured coatings are shown in Fig. 4. It is clear that columnar structure was formed in the coatings. With the shroud, the coating thickness was 2 μm, nearly twice that of 1.2 μm without the shroud.

The morphologies of nanoparticles or nanoclusters deposited with and without the shroud are shown in Fig. 5. The typical surface morphologies of YSZ coatings deposited with and without the shroud presented an island-like structure, in which each island was further composed of nanoparticles or nanoclusters.

4. Discussion

4.1 Effect of Powder Feeding on Plasma Condition

It was found from Fig. 3 that the plasma temperature was not significantly influenced by the powder feeding, although the heating, melting, evaporation, and even ionization of the YSZ powder must consume corresponding energy from the plasma jet. The powder feeding rate used in this study was 0.5 g/min, from which the arc

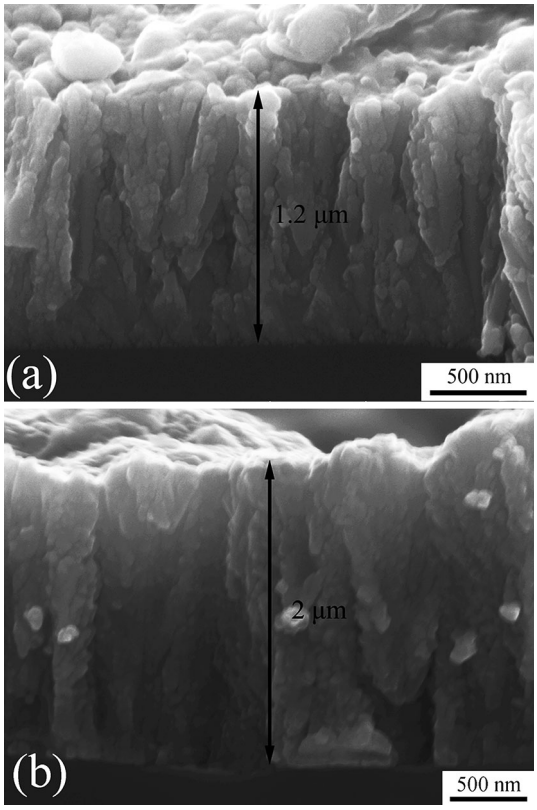

Fig. 4 Cross-sectional morphologies of fractured coatings: (a) without and (b) with shroud

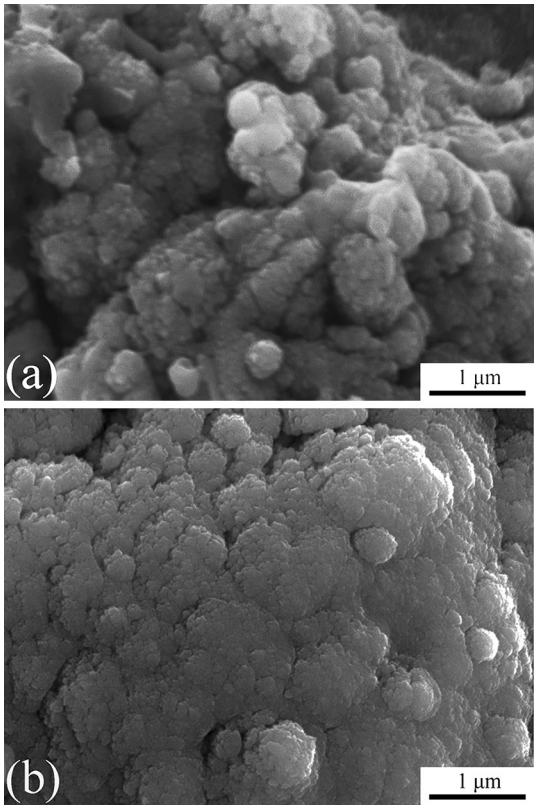

Fig. 5 Surface morphologies of coatings deposited (a) without and (b) with shroud

Table 2 Power for different heating states

	At melting point		At boiling point		
	No melting	Complete melting	No evaporation	Complete evaporation	Complete ionization to Zr^{1+}
Independent enthalpy, kJ/mol	182	87	39	624	660
Cumulative enthalpy, kJ/mol	182	269	308	932	1592
Cumulative power with powder, kW	0.012	0.018	0.021	0.063	0.108

power necessary for the different heating states was also calculated based on the literature (Ref 30). Table 2 presents the enthalpy values needed to achieve the individual thermodynamic states and the accumulated values of enthalpy and power for the powder. The specific heat capacity used to calculate the enthalpy of zirconia was taken as 0.0757 kJ/(K mol) (Ref 30). The net arc power of the plasma jet was 24 kW. The powder needs 0.018 kW power from solid to complete melting. It needs 0.063 kW power from solid to complete evaporation. If the powder is completely ionized into Zr^+ from solid, 0.108 kW power is needed. It can be concluded that the power to heat all the powder to ions was about 0.45% of the arc power of the plasma jet. The power used to evaporate all the powder was about 0.26% of the arc power of the plasma jet. Therefore, from the point of view of thermal energy, the plasma temperature was barely influenced by the powder feeding.

Besides high-energy ions and electrons, there are a much larger number of neutral species in the plasma jet. The heating of the YSZ powder before ionization mainly depends on the high-temperature neutral species, while the ionization of the spray powder must depend on high-energy electrons in the plasma jet. The atomic fraction of total zirconium and yttrium in the plasma jet can be calculated from Eq 3 as

$$MF = \frac{F_D \times 93\%/M_{ZrO_2} + 2 \times F_D \times 7\%/M_{Y_2O_3}}{F_{Ar}\rho_{Ar}/M_{Ar} + 2 \times F_{H_2}\rho_{H_2}/M_{H_2}}, \quad \text{(Eq 5)}$$

where MF is the atom fraction, F_D is the powder feeding rate (g/min), M_{ZrO2} and M_{Y2O3} are the molar mass of zirconia and yttria (g/mol), F_{Ar} and F_{H2} are the flow rate of argon and hydrogen (L/min), ρ_{Ar} and ρ_{H2} are the density of argon and hydrogen (g/L), and M_{Ar} and M_{H2} are the argon and hydrogen molar mass (g/mol).

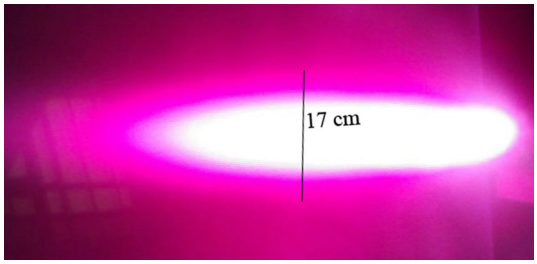

Fig. 6 Diameter of plasma jet without powder and shroud

For a powder feed rate of 0.5 g/min, the mole mass of ZrO_2 and Y_2O_3 is 122 and 226 g/mol. The flow rate of Ar and H_2 was 40 and 8 L/min. The density of argon and hydrogen was 1.784 and 0.0899 g/L. The mole mass of argon and hydrogen was 36 and 2 g/mol. The atomic fraction of YSZ in the plasma jet was about 0.15%. If the YSZ powder was all ionized, the number of yttrium and zirconium ions in the plasma jet was much lower than the electron number. Therefore, the powder barely influenced the electron number density.

4.2 Effect of Shroud on Plasma Condition and YSZ Vaporization

It can be seen from Fig. 6 that the diameter of the plasma jet was about 17 cm. The detection range of OES shown in Fig. 1 is about 300 mm. Therefore, the diameter of the plasma jet is included in the OES detection range. It was found that the electron number density without the shroud was larger than that with the shroud. The plasma jet is concentrated due to the restriction by the shroud. The collisions of species in the restricted plasma jet are intense. The low electron number density is probably due to recombination of electrons with ions during such intense collisions in the concentrated plasma jet. The energy released from such recombination was used to increase the plasma temperature. The powder is heated more effectively in the high-temperature plasma jet, resulting in more evaporation. The expansion of the plasma jet also results in a decrease of the electron number density.

4.3 Effect of Shroud on Coating Deposition

It can be concluded from the microstructure of the cross-section (Fig. 4) that the deposition rate of the coating without the shroud was about half that with the shroud. This means that the evaporation of the YSZ powder with the shroud was twice that without the shroud. The shrouded plasma torch makes the plasma jet concentrated, resulting in a greater ability to evaporate more powder.

The surface morphologies of coatings deposited with and without the shroud were not evidently different; they were all composed of nanoparticles or nanoclusters. Therefore, besides atoms in gas phase, the deposition can be contributed by clusters (Ref 31). The deposition behavior was not changed even though the evaporation capacity of the plasma jet with the shroud was greater than that without the shroud. This indicates that the use of a shroud is a simple but effective approach to improve powder heating and evaporation in PS-PVD.

5. Conclusions

YSZ coatings (7 wt.%) were deposited by PS-PVD using a shrouded torch, and the characteristics of the plasma jet were diagnosed using OES. The electron number density and plasma temperature were barely influenced by the powder feeding rate due to the much greater thermal energy of the plasma jet. Compared with the conventional torch, the shrouded torch resulted in a concentrated plasma jet having lower electron number density but higher plasma temperature. This is due to the greater recombination of high-energy ions and electrons, releasing energy to further heat the plasma in the limited space of the shroud. As a result, the powder evaporation capacity with the shrouded plasma was significantly improved compared with that without the shroud, resulting in twice the coating deposition rate. This indicates that the use of a shroud is a simple but effective approach to improve powder heating and evaporation in PS-PVD.

Acknowledgments

This research work was sponsored by the National Basic Research Program of China (2012CB625100, 2013CB035701), National Natural Science Foundation of China (51342003), National Program for Support of Top-notch Young Professionals, and Fundamental Research Funds for the Central Universities.

References

1. P. Carpio, E. Bannier, M.D. Salvador, R. Benavente, and E. Sanchez, Multilayer and Particle Size-Graded YSZ Coatings Obtained by Plasma Spraying of Micro- and Nanostructured Feedstocks, *J. Therm. Spray Technol.*, 2014, **23**(8), p 1362-1372
2. G.J. Yang, Z.L. Chen, C.X. Li, and C.J. Li, Microstructural and Mechanical Property Evolutions of Plasma-Sprayed YSZ Coating During High-Temperature Exposure: Comparison Study Between 8YSZ and 20YSZ, *J. Therm. Spray Technol.*, 2013, **22**(8), p 1294-1302
3. C.J. Li, Y. Li, G.J. Yang, and C.X. Li, Evolution of Lamellar Interface Cracks During Isothermal Cyclic Test of Plasma-Sprayed 8YSZ Coating with a Columnar-Structured YSZ Interlayer, *J. Therm. Spray Technol.*, 2013, **22**(8), p 1374-1382
4. M.A. Ali, H. Kim, K. Jeong, H. Soh, and J. Lee, Effects of Solvents on Poly (3, 4-Ethylenedioxythiophene) (PEDOT) Thin Films Deposited on a (3-Aminopropyl) Trimethoxysilane (APS) Monolayer by Vapor Phase Polymerization, *Electron. Mater. Lett.*, 2010, **6**(1), p 17-22
5. Y. Zhang, D.E. Mack, M.O. Jarligo, X. Cao, R. Vaßen, and D. Stover, Partial Evaporation of Strontium Zirconate During Atmospheric Plasma Spraying, *J. Therm. Spray Technol.*, 2009, **8**(4), p 694-701

6. Y.P. Wan, J.R. Fincke, S. Sampath, V. Prasad, and H. Herman, Modeling and Experimental Observation of Evaporation from Oxidizing Molybdenum Particles Entrained in a Thermal Plasma Jet, *Int. J. Heat Mass Transf.*, 2002, **45**, p 1007-1015
7. S. Rezanka, G. Mauer, and R. Vaßen, Improved Thermal Cycling Durability of Thermal Barrier Coatings Manufactured by PS-PVD, *J. Therm. Spray Technol.*, 2014, **23**(1–2), p 182-189
8. G. Mauer, A. Hospach, N. Zotov, and R. Vaßen, Process Conditions and Microstructures of Ceramic Coatings by Gas Phase Deposition Based on Plasma Spraying, *J. Therm. Spray Technol.*, 2013, **22**(2–3), p 83-89
9. K.V. Niessen and M. Gindrat, Plasma Spray-PVD: A New Thermal Spray Process to Deposit Out of the Vapor Phase, *J. Therm. Spray Technol.*, 2011, **20**(4), p 736-743
10. K.V. Niessen, M. Gindrat, and A. Refke, Vapor Phase Deposition Using Plasma Spray-PVD, *J. Therm. Spray Technol.*, 2010, **19**(1–2), p 502-509
11. K.V. Niessen, G. Eschendorff, M. Gindrat, and A. Refke, Advanced TBC Systems by Vapor Deposition Using LPPS Thin Film, In *Proceedings of the ASME Turbo Expo 2008: Power for Land, Sea and Air,* Berlin, Germany, 2008, pp 263-268
12. T. Yoshida, Toward a New Era of Plasma Spray Processing, *Pure Appl. Chem.*, 2006, **78**(6), p 1093-1107
13. A. Hospach, G. Mauer, R. Vaßen, and D. Stover, Columnar-Structured Thermal Barrier Coatings (TBCs) by Thin Film Low-Pressure Plasma Spraying (LPPS-TF), *J. Therm. Spray Technol.*, 2011, **116**(1–2), p 116-120
14. K.V. Niessen and M. Gindrat, Vapor Phase Deposition Using a Plasma Spray Process, *J. Eng. Gas Turb. Power.* 2011, 133, p 061301-1-7
15. G. Mauer, Plasma Characteristics and Plasma-Feedstock Interaction Under PS-PVD Process Conditions, *Plasma Chem. Plasma Process.*, 2014, **34**(5), p 1171-1186
16. G.R. Kornblum and L. de Galan, Spatial Distribution of the Temperature and the Number Densities of Electrons and Atomic and Ionic Species in an Inductively Coupled RF Argon Plasma, *Spectrochim. Acta B*, 1977, **32**(2), p 71-96
17. N. Furuta, Y. Nojiri, and K. Fuwa, Spatial Profile Measurement of Electron Number Densities and Analyte Line Intensities in an Inductively Coupled Plasma, *Spectrochim. Acta B.*, 1985, **40**(3), p 423-434
18. J.F. Alder and J.M. Mermet, A Spectroscopic Study of Some Radio Frequency Mixed Gas Plasmas, *Spectrochim. Acta B.*, 1973, **28**(11), p 421-433
19. M. Gindrat and A. Refke, Process Characterization of LPPS Thin Film Processes with Optical Diagnostics, *Thermal Spray*, 2007, p 826-831
20. G. Mauer and R. Vaßen, Plasma Spray-PVD: Plasma Characteristics and Impact on Coating Properties, *J. Phys. Conf. Ser.*, 2012, **406**, p 1-12
21. H.J. Kim and S.H. Hong, Comparative Measurements on Thermal Plasma Jet Characteristics in Atmospheric and Low Pressure Plasma Sprayings, *IEEE Trans. Plasma Sci.*, 1995, **23**(5), p 852-859
22. Y.K. Ke and H.R. Dong, *Handbook of Analytical Chemistry Third Fascicle Spectrum Analysis*, Chemical Industry Press, Beijing, 1998
23. S. Pellerin, K. Musiol, B. Pokrzywka, and J. Chapelle, Stark Width of 4s-4p ArI, Transition (696.543 nm), *J. Phys. B At. Mol. Opt.*, 1996, **29**, p 3911-3924
24. A.A. Ovsyannikov and M.F. Zhukov, *Plasma Diagnostics*, Cambridge International Science, Cambridge, 1995
25. D.R. Qiu, *The Atomic Spectrum Analysis*, Fudan University Press, Shanghai, 2002
26. G.A. Odintsova and E.P. Vaulin, Excitation Temperature and Gas Temperature in Supersonic Low-Density Flows, *J. Appl. Spectrosc.*, 1967, **7**, p 507-508
27. http://physics.nist.gov/PhysRefData/ASD/lines_form.html. Accessed 10 May 2014
28. C.K. Zheng, *Plasma Physics*, Peking University Press, Beijing, 2009
29. H.R. Griem, *Plasma Spectroscopy*, McGraw-Hill, New York, 1964
30. J.A. Dean, *Lange's Handbook of Chemistry*, Science Press and McGraw-Hill Education (Asia) Co, Beijing, 2003
31. Q.Y. Chen, C.X. Li, J.Z. Zhao, G.J. Yang, and C.J. Li, Microstructure of YSZ coatings deposited by PS-PVD using 45 kW shrouded plasma torch, *Mater. Manuf. Process.* (in press)